



Obrabotka metallov -

Metal Working and Material Science

Journal homepage: http://journals.nstu.ru/obrabotka_metallov



Numerical study of titanium alloy high-velocity solid particle erosion

Evgeniy Strokach^{a, *}, Gleb Kozhevnikov^b, Aleksey Pozhidaev^c, Sergey Dobrovolsky^d

Moscow Aviation Institute (National Research University), 4 Volokolamskoe shosse, Moscow, 125993, Russian Federation

^a <https://orcid.org/0000-0001-5376-1231>, evgenij.stroksch@mai.ru; ^b <https://orcid.org/0009-0001-4622-7476>, kozhevnikov.mai@yandex.ru;
^c <https://orcid.org/0000-0002-7667-5392>, pozhidaev.mai@xmail.ru; ^d <https://orcid.org/0000-0002-1884-1882>, dobrovolskiy_s@mail.ru

ARTICLE INFO

Article history:

Received: 15 September 2023

Revised: 29 September 2023

Accepted: 28 October 2023

Available online: 15 December 2023

Keywords:

Erosion wear

Numerical simulation

Solid particles

Ansys FLUENT

Shape factor

Ti6Al4V

CFD

Solid particle erosion

GEKO

Turbulence model

RANS erosion study

Funding

The research was funded by the ministry of Science and Higher Education of the Russian Federation, grant number FSFF-2023-0006.

Acknowledgements

Research was partially conducted at core facility "Structure, mechanical and physical properties of materials".

ABSTRACT

Introduction. Predicting solid particle erosion (*SPE*) in gaseous flow and managing its intensity is still a relevant problem in mechanical engineering. It requires the development of a general modeling methodology, which also depends upon many special cases studying various physical processes. Such studies should also include verification analysis, process parameters and model sensitivity studies. Mainly computational fluid dynamics and finite element analysis (and mesh-free methods such as smooth particle hydrodynamics or similar) are used to simulate the erosion process. Papers focused on *CFD* simulation of solid particle erosion of metal alloys are widely presented, but most of it is associated with relatively low or medium particle velocities (< 100–150 m/s) and is close to uniform diameter distribution. This paper presents a *CFD* study of *Ti₆Al₄V* titanium alloy *SPE* at relatively high particle velocities and sufficiently non-uniform unimodal particle diameter distribution. The paper also studies the turbulence model influence and particle shape effect which appears as a "shape factor" coefficient in the particle drag model. **Methods.** The heterogenous flow simulation was based on the *Reynolds-averaged Navier-Stokes* formulation, where the particles, according to *Euler-Lagrange* formulation, were simulated as mathematical points with corresponding properties. The influence of turbulence models, such as *k*-epsilon standard, *RNG k*-epsilon, and a relatively new Generalized equation *k*-omega (*GEKO*) model and its coefficients were also studied. *Oka* and *DNV* erosion models were also compared based on the general sample mass loss and more specific erosion intensity profile criterions. The simulation results were compared to the lab-scale experimental results. **Results and discussion.** It is shown that neither erosion intensity profile or sample mass loss do not depend upon the turbulence model choice or *GEKO* parameters variation. As expected, erosion is dependent on the erosion model and its coefficients. A notable influence of the shape factor is shown. As the drag coefficient increased due to the particle shape, the erosion intensity decreased and the erosive profile on the surface also changed due to the changing velocity and diameter distribution of the heterogenous flow. It is expected that such results would be useful not only for erosion prediction in all areas of mechanical engineering, but also for wear management in mechanical assemblies and shot peening / shot peen forming management and simulation.

For citation: Strokach E.A., Kozhevnikov G.D., Pozhidaev A.A., Dobrovolsky S.V. Numerical study of titanium alloy high-velocity solid particle erosion. *Obrabotka metallov (tekhnologiya, oborudovanie, instrumenty) = Metal Working and Material Science*, 2023, vol. 25, no. 4, pp. 268–283. DOI: 10.17212/1994-6309-2023-25.4-268-283. (In Russian).

Introduction

Solid particle erosion, particularly in the gas flow, is a prevalent issue across aerospace, energy, automotive, and various other sectors. Experimentation on different particle materials, surface and coating materials, flow conditions, particle characteristics, and more has generated a wealth of research on this

* Corresponding author

Strokach Evgeniy A., Ph.D. (Engineering), leading engineer

Moscow Aviation Institute (National Research University),

4, Volokolamskoe shosse,

125993, Moscow, Russian Federation

Tel.: +7 (916) 338-63-66, e-mail: evgenij.stroksch@mai.ru



phenomenon. Many empirical-analytical methods were developed to estimate engineering erosion rates. These include the *Finnie*, *Bitter*, *Oka*, *Tabakoff* approaches, among others. These methods were applied and continuously improved over time. Recently, numerical modelling methods using both *CFD* (computational fluid dynamics) and *FEA* (finite element analysis) as well as *SPH* (smooth particle hydrodynamics) and its derivatives, which allow for the study of micro-level processes [1, 9–14], have made significant progress.

Previously, the text provided a brief overview of erosion modeling methods, examining some works that applied *CFD* and *FEA* [8]. One of the most commonly used methods for modeling and verification is a system comprising one or more 90° bent channels that accelerates particles using a carrier phase, typically air, which in turn erodes the surface [2, 3, 15]. When modelling particle motion using *CFD*, the *Euler-Lagrange* approach is commonly used to depict particle groups as mathematical points with known mass, material and dimensions [16–18]. In publications, authors compare and suggest various turbulence models, with calculations typically based on the *Reynolds-averaged Navier-Stokes* equation system, alongside semi-empirical erosion models, depending on the specific issue.

Shinde et al. [1] conducted an excellent review of the use of *CFD* and empirical-analytical models. The authors establish that *CFD* has a high level of accuracy for various issues and note the need for new empirical-analytical relationships and estimating particle angle of incidence, which relies on carrier phase.

The findings regarding erosion wear caused by particles in fluid flow that cannot be compressed, known as “slurry erosion”, are relevant to erosion in a gaseous medium as well. Therefore, the *E/CRC* group’s representatives, *H. Arabnejad* [19] and *A. Mansouri* [20], have created and confirmed empirical-analytical connections by separating the types of wear: deformation and abrasion, which was previously suggested by *Bitter* [6, 7]. These models involve numerous parameters, covering aspects such as particle shape, flow conditions, and surface material. Overall, these relationships hold great potential for modelling erosion in gaseous media.

The contemporary examination of erosion by particles involves *FEA* and *SPH* modelling. This approach was scrutinized in multiple reviews, including those by *R. Tarodiya* and *A. Levy*, *A. Krella*, *V. Bonu* and *H. Barshilia*, *A. Fardan* [9–12]. Modern works are focused on refining material models that describe plastic behavior and fracture conditions, as well as the influence of sample temperature, coatings effectiveness, particle shape and size. Additionally, these works also take into account the conditions of particle flow, including velocities, mutual collision, angles of incidence, and particle rotation. This became possible due to the ability to model particle-surface collisions explicitly [21–28].

Despite significant effort to develop a methodology for modelling the erosion caused by solid particles on different materials and under various conditions, there is currently no universally applicable methodology to describe both micro- and macro-level processes. However, ongoing studies examine specific phenomena and the impact of mathematical models on material erosion in particular cases.

This paper is focused on the modelling of surface erosion in a popular titanium alloy (Ti_6Al_4V) caused by SiO_2 particles flowing in air. Accurate gas flow description is crucial in this modelling process, particularly when using the most common *Reynolds-averaged Navier-Stokes* equations (*RANS*) approach that requires the selection of a turbulence model. *CFD* erosion modelling involves estimating the surface material entrainment rate as a function of particle impact conditions. Typically, empirical-analytical methods are used, relying on empirically-based coefficients for a narrow range of conditions. These coefficients may require adjustment, and it is necessary to evaluate the model sensitivity to its variation.

Many studies analyzed the impact of turbulence models in *CFD* modelling of the particle erosion process. However, most of these studies were conducted at low velocities of heterogeneous mixture flowing on the surface (less than 150–200 m/s) and did not incorporate the relatively new generalized equation *k-omega* (*GEKO*) model [29–31]. The model can be calibrated using multiple coefficients to mimic a particular issue while sustaining coherence and physicality. In this paper, the *GEKO* model is analyzed in comparison to the commonly used *k-epsilon* standard and *RNG*, with particular emphasis on its unique features.

Additionally, current publications primarily examine erosion caused by particles of a singular or limited diameter range. However, considering the non-uniform distribution of particles can significantly affect the

formation of a heterogeneous jet, ultimately altering the wear profile of the surface. This study introduces particles have a range of 2–63 μm , with a preference towards smaller diameters.

Thus, this paper aims to examine the approach to *CFD* modelling of a particular scenario in which a high-velocity, heterogeneous jet with a significantly non-uniform particle size distribution flows onto a Ti_6Al_4V sample. Due to the limited space of this paper, the goals include studying how the choice of turbulence models and its adjustment coefficients, the selection of erosion models and its adjustment coefficients, as well as the influence of particle shape, affect the modelled wear rate. In addition, the selected approach's performance is evaluated by comparing integral values of the calculated and experimental erosion rates, as well as by comparing the calculated specific erosion rate profiles and the experimental material entrainment profile.

Research methodology

Experiment

For the purposes of this study, we utilized a laboratory experimental bench to examine surface erosion under the influence of heterogeneous flow. The operational principle involved introducing quartz particles into the mixing chamber, from where a mixture of gas (in this instance – air) and particles then was feed into the accelerator. The accelerator, which is a *Laval* nozzle, enabled the heterogeneous flow to accelerate under the action of pressure difference and impinge on the stationary sample. The significant parameters that define the experimental point were the pressure at the accelerator inlet and the initial gas temperature. This configuration enables the examination of wear under various particle flow angles, temperatures, and velocities. The observed test outcomes were the shape of the crater and the loss of the sample material. These results aid in quantifying the wear rate.

The flow rate of particles at each experimental point was $7.64e^{-6}$ kg/s for 5 minutes, with a temperature of 140 °C and accelerator pressure of 5.75 bar. The accelerator cut-off was positioned 20 mm away from the sample at a 90° angle to the accelerator position. Fig. 1 displays the size distribution of SiO_2 particles. The spectrum was mainly dominated by minute fractions, with the highest equivalent particle diameter of 63 μm .

Problem formulation and geometric model

Owing to insufficient experimental data on the flow and particle velocity distribution in accelerator regions during the flow onto the sample, the entire accelerator had to be modelled. This was done in order to adequately take into account the variables when estimating the erosion rate. To achieve this, an integral

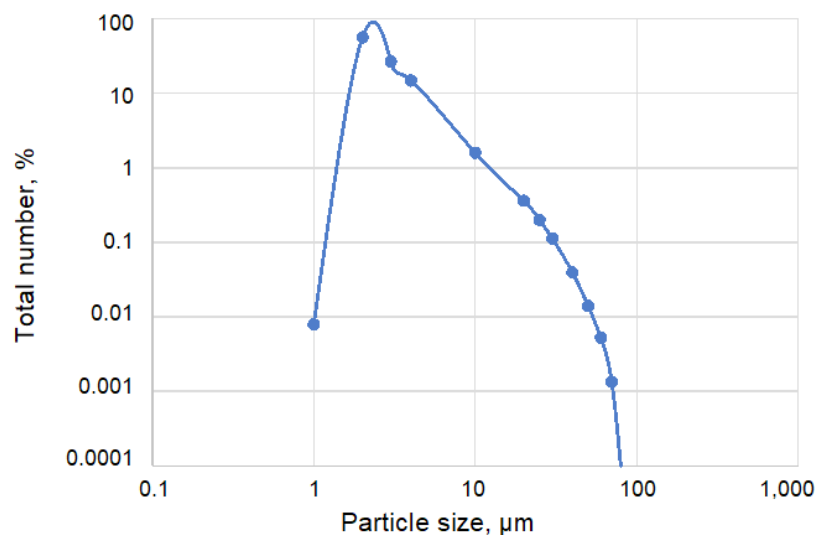


Fig. 1. Particle size distribution

computational domain was instituted within the accelerator, as well as between the nozzle slice of the tube and the eroded surface. Fig. 2 displays a general view of the accelerator tube with the nozzle. A mixture of particles and air enters the *Laval* nozzle, accelerates, and exits through the tube onto a sample comprised of titanium alloy Ti_6Al_4V .

Due to the axisymmetric nature of the problem, the two-phase flow area can be depicted in a two-dimensional axisymmetric format, which boosts the accuracy of the calculation and reduces computational resources. The computational domain was entirely modelled using two mesh regions, namely the accelerator, and the flow area between the accelerator and the sample. A block mesh with a structured design and a high dimensionless distance y^+ near the erodible surface was created in *ICEM CFD* software. This was due to the utilization of a scaled wall function for boundary layer modelling. The labelled schematic diagram with the designation of the types of boundary conditions (*BCs*) is shown in fig. 3.

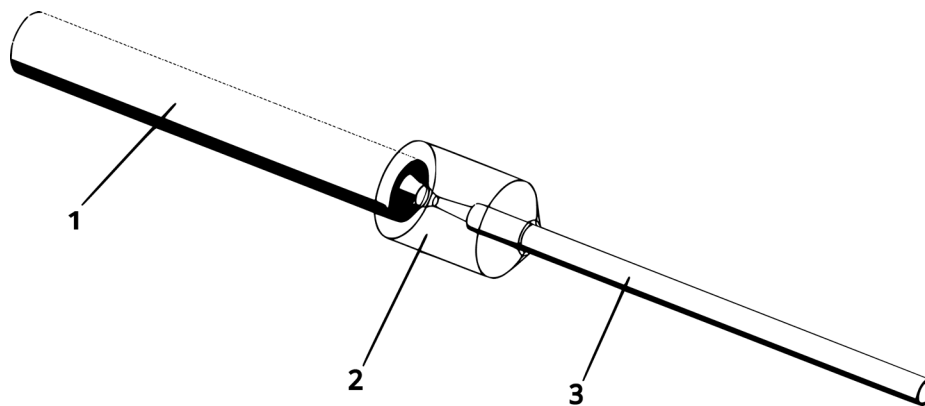


Fig. 2. Flow accelerator model: mixer (1), converging part (2), diverging part (3)

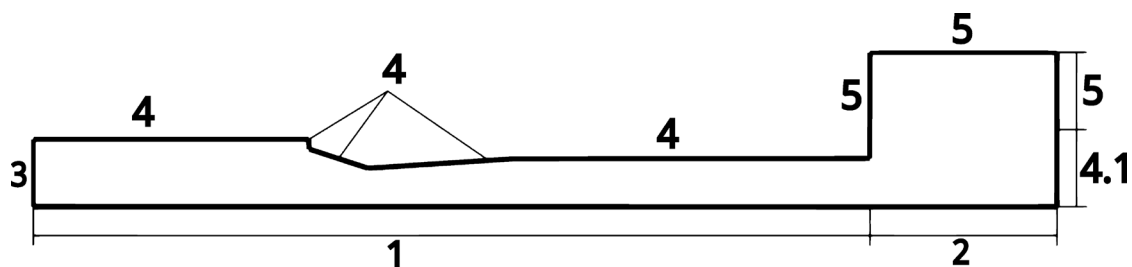


Fig. 3. 2d axisymmetrical schematic diagram and boundary conditions: accelerator area (1); outflow from accelerator to sample (2); inlet boundary condition (air + particle initialization area) (3); wall boundary condition (4); sample wall *BC* (4.1); pressure outlet boundary condition (5)

Physical Models/ Grid Convergence Study

The model in question is based on using *Reynolds-averaged Navier-Stokes* equations to describe the movement of the carrier phase – air (ideal gas). To average the results, considering turbulent phenomena through a turbulence model is necessary, the choice of which can substantially affect the outcomes. A specific evaluation of both models and its coefficients' sensitivity is required. Next, we will discuss the impact of models founded on equations for turbulent kinetic energy (k), its dissipation rate (ϵ), and models founded on k and specific dissipation rate (ω): k -epsilon standard, k -epsilon *RNG*, and *Generalised equation k-omega (GEKO)* [29–31]. The k -epsilon standard model serves as the foundation for numerous turbulence models intended to explain phenomena within the flow core. *RNG* is deemed to provide increased precision for high velocity gradient, swirling flows [30]. *GEKO* is a new model, based on k and ω , which uniquely

maintains its integrity even when adjusting its tuning coefficients. However, its full documentation remains inaccessible. Put simply, the user can modify the model's behavior across a broad range of solutions without concern for physical implications. The fundamental equations are provided below. *GEKO* model equations from [29–32]:

$$\frac{\partial(\rho k)}{\partial t} + \frac{\partial(\rho u_j k)}{\partial x_j} = \frac{\partial}{\partial x_j} \left[\left(\mu + \frac{\mu_t}{\sigma_k} \right) \frac{\partial k}{\partial x_j} \right] + P_k - C_\rho \rho k \omega; \quad (1)$$

$$\frac{\partial(\rho \omega)}{\partial t} + \frac{\partial(\rho u_j \omega)}{\partial x_j} = \frac{\partial}{\partial x_j} \left[\left(\mu + \frac{\mu_t}{\sigma_k} \right) \frac{\partial \omega}{\partial x_j} \right] + P_k C_{\omega 1} F_1 \frac{\omega}{k} - F_2 C_{\omega 2} \rho \omega^2 + C D F_3 \rho. \quad (2)$$

The functions $F1$, $F2$ and $F3$ [29–31] implement the C_{mw} , C_{sep} and C_{mw} coefficients, respectively. According to the authors, the C_{mw} coefficient is designed to modify the model's behavior within the boundary layer and near the wall, although its influence is expected to be minimal given the use of the near-wall function. The C_{jet} coefficient, although mentioned in the documentation, is not the primary parameter for enhancing model performance. However, it can be beneficial for circular concentric flows. Given the cylindrical nozzle of the accelerator, this coefficient may have an impact under certain conditions. Ultimately, C_{sep} is deemed the most dominant coefficient, with the aim to enhance performance for significant adverse pressure gradients and to resolve regions with laminar-turbulent transition. Previously, in the case of reacting flow [32], it was found that C_{sep} was the most crucial coefficient for pressure and heat flux criteria, and reducing C_{sep} brought *GEKO* performance closer to the k -epsilon model. Additionally, in earlier tests for heterogeneous flow with relatively low velocities within the pipe, the *GEKO* model and its parameters' variations had only a minor impact on the velocity and wear pattern in the pipe elbow [33].

The *Euler-Lagrangian* approach, which is well established for such problems [2, 3, 8, 15–19], was used to model the particulate matter. During the accelerator inlet BC calculations, the pressure and temperature were set to match the experimental values for the point being investigated. Solid particles were also introduced, flowing at a rate of $7.65e^{-6}$ kg/s, based on the experimental number distribution and a zero velocity assumption (due to a lack of information regarding particle velocity in the precritical section of the accelerator). The particle velocity was made equal to the flow velocity, and a drag law based on particle sphericity was established. For modelling particle wear in *CFD*, an erosion model must be applied to the erodible surface. Empirical-analytical models are often employed to relate the material removal rate to the flowing particle parameters, including size, velocities, and angle of incidence.

When performing these calculations, several empirical coefficients are utilized, generally chosen based on the specific materials being used. Among the most widely employed commercial software is Ansys *FLUENT*, with the *Oka* [34] model being one of its most frequently applied components, serving as a cornerstone for investigating grid convergence and turbulence model impact.

Grid convergence was investigated by performing calculations on five grids of different dimensionality using the *Oka* model, the k -epsilon *Standard Shear-Stress Transport Turbulence Model*, and a turbulent *Prandtl* number of 0.85. A design point of 5.75 bar at 140 °C was utilized.

After evaluating the total specific erosion criterion, a mesh with 1.65 million hexahedral cells in the region between the accelerator and the sample was chosen. The velocity profile criterion was selected to assess the accelerator mesh in the expulsion region. The accelerator area's final computed grid consisted of 190,000 cells.

Results and discussion

It is evident that the rate of surface erosion is reliant on the distribution of particle velocities and incidence angles, which is linked to the velocity profile at the outflow from the accelerator. Fig. 4 displays a representative image of the flow at the accelerator outflow and surface flow using the k -epsilon turbulence model. In the normal direction of high-speed flow near the wall, velocity sharply decreases. Nonetheless,

a local region of flow acceleration forms, flowing around the braking region. The heterogeneous flow accelerator creates a high-velocity jet, which promotes the downstream airflow's ejection and its acceleration. As a consequence, a zone of opposing currents is created, which has no impact on the erosion process anymore, given its significant distance from the eroded surface (refer to fig. 4, located at the base of the high-velocity jet, in the center).

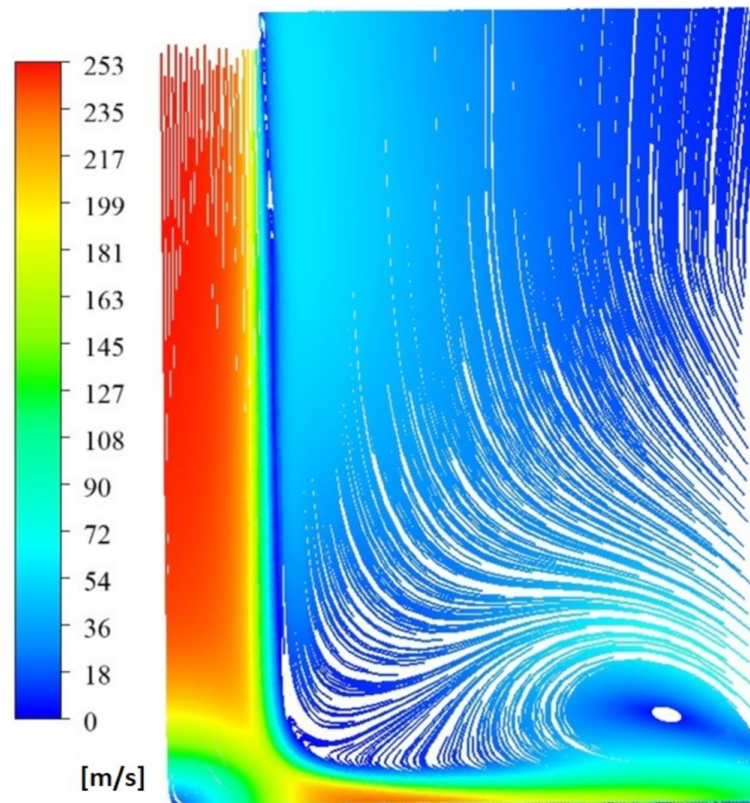


Fig. 4. High-velocity flow impacting sample surface

To construct an erosion rate analysis and develop model comparisons, we utilised the specific erosion wear criterion which was determined by calculating the ratio of mass that was removed to the mass of particles present in each cell on the sample surface (specifically region 4.1 in fig. 3). The turbulence model's impact along the length of the sample, on the radius of the wear spot is shown in fig. 5 (where the centre of the spot is identified as 0 mm).

The limited effect of the turbulence model is evident, which is caused by the similar distribution of flow velocities and turbulent viscosity (which is determined by the turbulence model), as shown earlier for the reacting flow [32].

As previously mentioned, the *GEKO* model provides unique opportunities to adjust the model coefficients. Figs. 6–8 demonstrate the effect of the *GEKO* model tuning parameters – C_{sep} , C_{nw} , C_{jet} .

It is apparent that the primary adjustment coefficients of the *GEKO* model have minimal or no impact on erosion wear when varied within a broad range, even when compared to the overall influence of the turbulence model.

The impacts of the erosion model were evaluated using two of the most widely used models, *Oka* [30, 34] and *DNV* [30, 35]. The *Oka* model was utilized through the following formulation:

$$E = E_{90} \left(\frac{V}{V_{ref}} \right)^{k_2} \left(\frac{d}{d_{ref}} \right)^{k_3} f(\gamma), \quad (3)$$

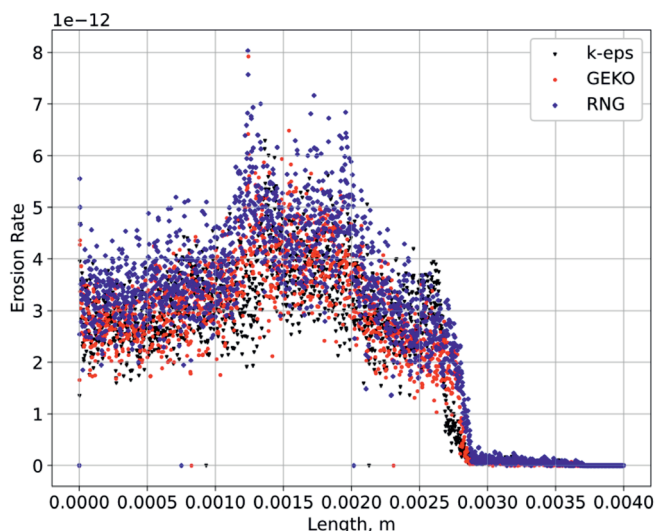


Fig. 5. The effect of turbulence models

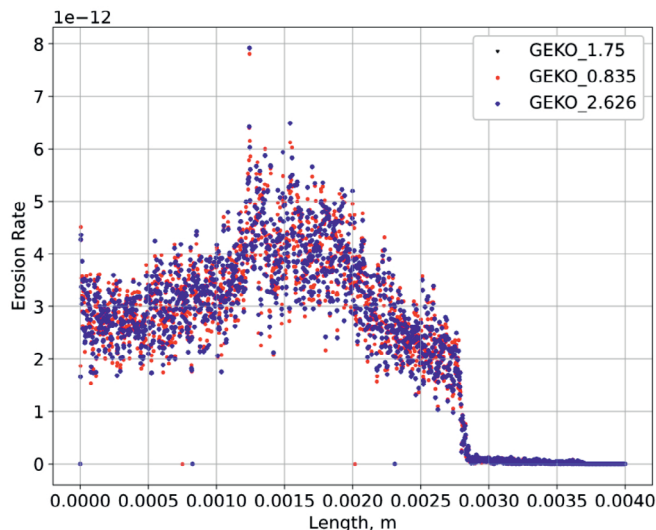


Fig. 6. The effect of C_{sep} GEKO coefficient

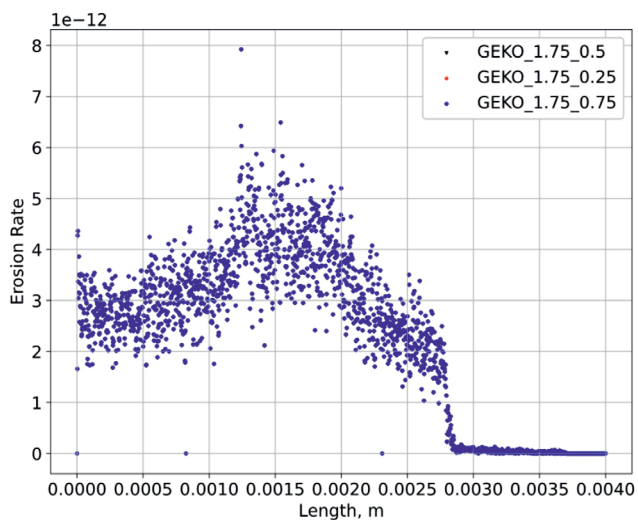


Fig. 7. The effect of C_{mw} GEKO coefficient at C_{sep} 1.75

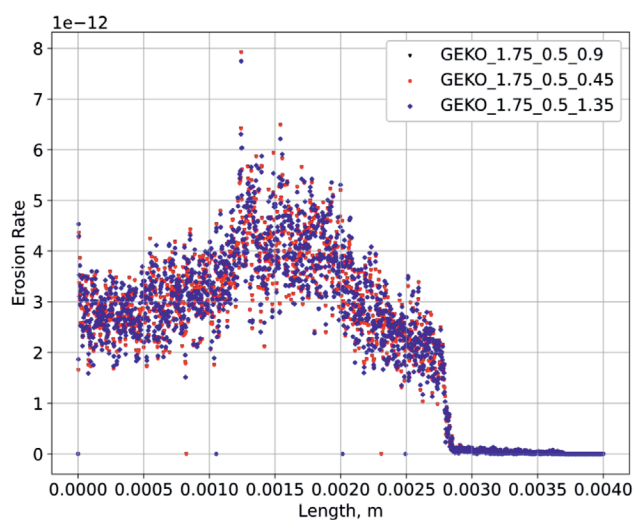


Fig. 8. The effect of C_{jet} GEKO coefficient at C_{sep} 1.75 and C_{mw} 0.5

where E_{90} is the reference erosion rate at a particle incidence angle of 90° ; V is the particle velocity; V_{ref} is the reference velocity; d is the particle diameter; D_{ref} is the reference diameter; k_2 and k_3 are the model coefficients; $f(\gamma)$ is a function of angle defined as:

$$f(\gamma) = (\sin \gamma)^{n_1} (1 + H_v(1 - \sin \gamma))^{n_2}, \tag{4}$$

where γ – represents the angle of incidence of the particle (in radians); H_v denotes the Vickers hardness coefficient (in GPa); n_1 and n_2 are constants.

DNV model is formulated as:

$$E = \dot{m}_p K U_p^n f(\alpha), \tag{5}$$

where \dot{m}_p is erodent mass flow rate; K , n are constants; $f(\alpha) = \sum -1^{i+1} A_i \left(\frac{\alpha\pi}{180}\right)^i$, and its coefficients are presented in table 1.

The coefficients of empirical-analytical models are dependent on the material and experimental conditions. In order to examine the independent parameters of the *Oka* model, the coefficients were established



Table 1

DNV model coefficients

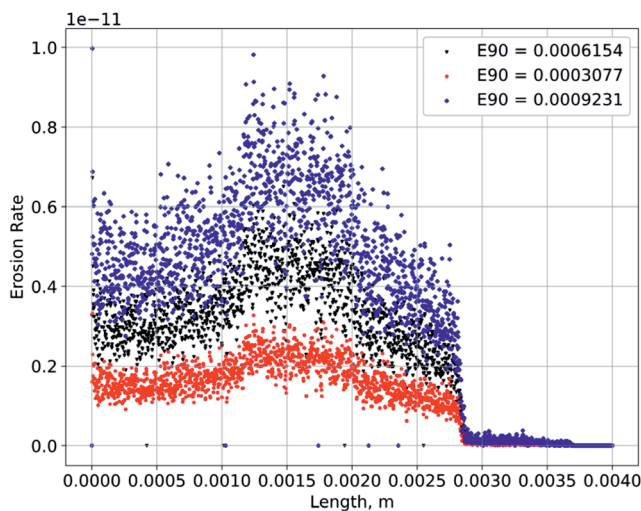
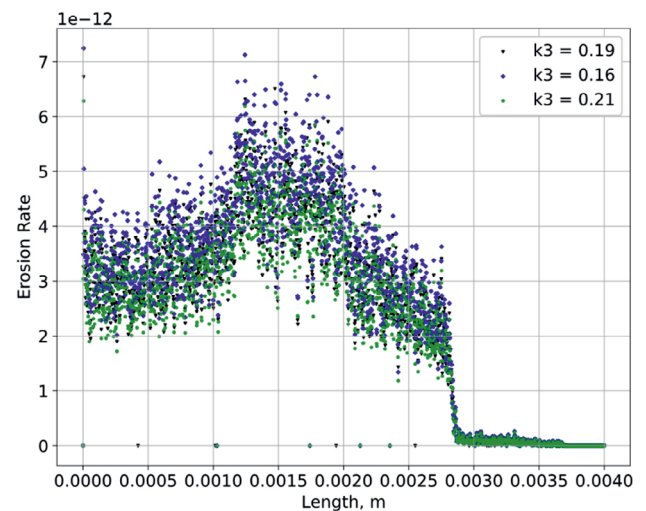
A_1	A_2	A_3	A_4	A_5	A_6	A_7	A_8
9.37	42.295	110.864	175.804	170.137	98.398	31.211	4.17

utilizing the *Vickers* microhardness of the erodible material and following the guidelines stated in [36], while E_{90} is a tuned coefficient. Table 2 and figs. 9, 10 present a study of E_{90} and k_3 coefficients' influence, The calculated erosion rate termed "*ER sim*" is compared with the experimental "*ER exp*" from two identical experiments. k_3 is a coefficient by the normalized diameter, while it is obvious that k_2 , being a factor by normalized velocity, and angle function would be influential.

Table 2

The effect of *Oka* parameters

No.	<i>Oka</i>								<i>ER sim</i>
	E_{90}	HV (GPa)	n_1	n_2	k_2	k_3	D_{ref}	Vel_{ref}	
1	$6.154e^{-4}$	0.35	0.613	6.439	2.21	0.19	0.00326	104	$6.322e^{-4}$
2	$3.077e^{-4}$	0.35	0.613	6.439	2.21	0.19	0.00326	104	$3.161e^{-4}$
3	$9.231e^{-4}$	0.35	0.613	6.439	2.21	0.19	0.00326	104	$1.057e^{-3}$
4	$6.154e^{-4}$	0.35	0.613	6.439	2.21	0.16	0.00326	104	$6.88e^{-4}$
5	$6.154e^{-4}$	0.35	0.613	6.439	2.21	0.21	0.00326	104	$5.977e^{-4}$
6	$4e^{-3}$	0.35	0.613	6.439	2.21	0.19	0.00326	104	$4.239e^{-3}$
7	$8e^{-3}$	0.35	0.613	6.439	2.21	0.19	0.00326	104	$8e^{-3}$
8	$5e^{-3}$	0.35	0.613	6.439	2.21	0.19	0.00326	104	$5.046e^{-3}$
<i>ER exp</i>									$4.43e^{-3}$
									$3.16e^{-3}$


 Fig. 9. The effect of E_{90} coefficient

 Fig. 10. The effect of k_3 coefficient

The coefficient's k_3 effect is small compared to E_{90} (E_{ref}) and similar to that of the turbulence model.

The Ti_6Al_4V (Ti_6Al_4V analogue) DNV model parameters are taken from [37]. The influence of the linear coefficient K and power n can be seen in table 3 and figs. 11, 12.

Table 3

The effect of DNV parameters

No.	DNV		$ER sim$
	K	n	
1	$2e^{-9}$	2.6	$5.919e^{-4}$
2	$1e^{-9}$	2.6	$2.959e^{-4}$
3	$3e^{-9}$	2.6	$8.878e^{-4}$
4	$2e^{-9}$	3.9	$7.044e^{-4}$
$ER exp$			$4.43e^{-03}$
			$3.16e^{-03}$

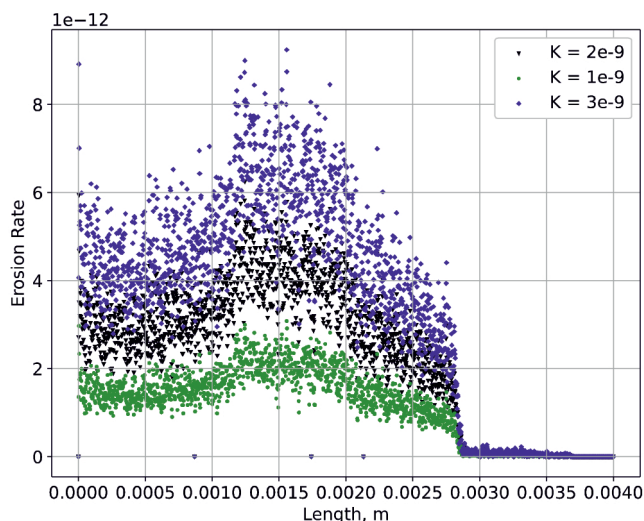


Fig. 11. The effect of K coefficient along the sample

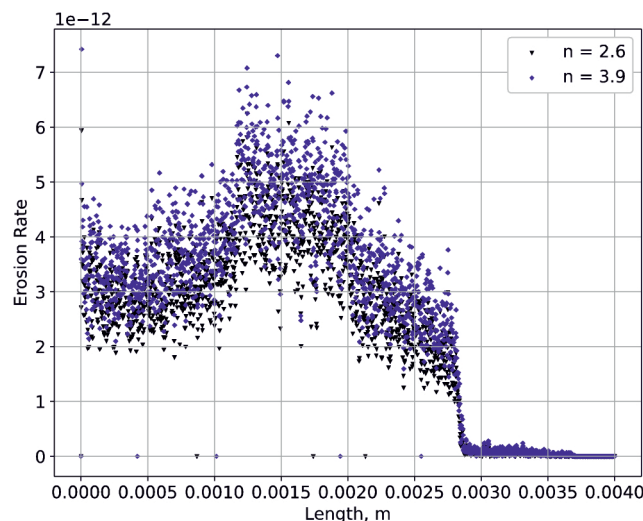


Fig. 12. The effect of n coefficient along the sample

As can be observed, the linear coefficient has a much higher effect in contrast to the exponent. Also, notable erosion rate values are reached at approximately 2.7 mm from the center of the erosion crater, decaying to zero at ≈ 3.7 mm. Similar erosion area (fig. 13) is observed on the samples, which qualitatively confirms the simulation results. On the contrary, a mismatch between simulated erosion maximum along the sample length and the crater profile can be seen. This issue is discussed further.

Motion of a particle is defined by the resultant of the acting forces. Drag force has a high effect, which depends upon the medium properties, particle velocity, its size and shape. The model used here is able to consider particle non-sphericity by means of a shape factor coefficient (SF). As other meaningful parameters are specified preliminary, the particle shape influence and its description by an additional coefficient are still to be studied.

The drag coefficient accounting for particle non-sphericity is defined as presented by Haider and Levenspiel [30, 38]:

$$C_D = \frac{24}{Re_{sph}} \left(1 + b_1 Re_{sph}^{b_2} \right) + \frac{b_3 Re_{sph}}{b_4 + Re_{sph}}; \tag{6}$$

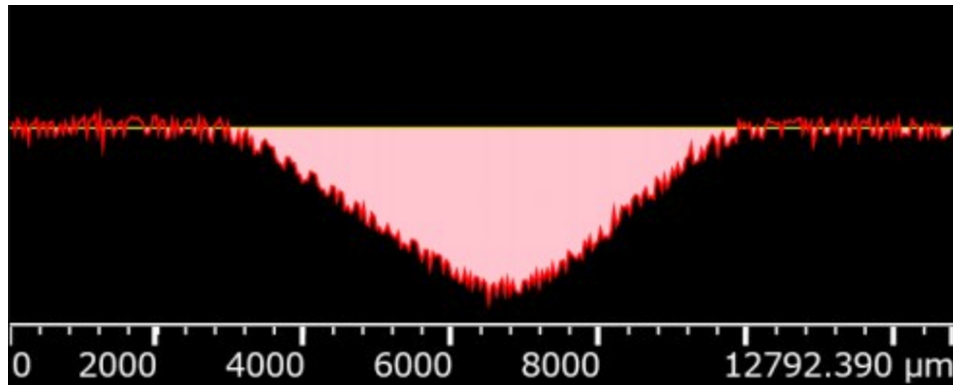


Fig. 13. Typical wear surface after testing

where

$$b_1 = \exp(2.3288 - 6.4581\varphi + 2.4486\varphi^2);$$

$$b_2 = 0.0964 + 0,5565\varphi;$$

$$b_3 = \exp(4.905 - 13.8944\varphi + 18.4222\varphi^2 - 10.2599\varphi^3);$$

$$b_4 = \exp(1.4681 + 12.2584\varphi - 20.7322\varphi^2 + 15.8855\varphi^3);$$

φ is a non-spherical shape constant;

$$\varphi = s/S,$$

where s is the surface area of a sphere having the same volume as a particle; S is the particle surface area.

The spherical drag coefficient was determined according to Morsi and Alexander [30, 39]:

$$C_D = a_1 + \frac{a_2}{Re} + \frac{a_3}{Re^2}, \quad a_1, a_2, a_3 - \text{constants.}$$

An additional study using *Oka* erosion model was conducted to estimate the influence of shape factor, which is presented in fig. 14.

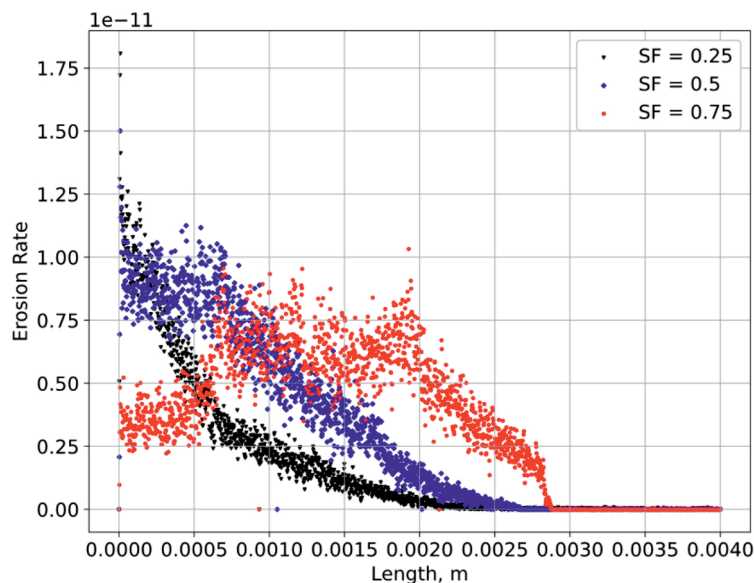


Fig. 14. The effect of the “shape factor” (for *Oka* coefficients $E_{90} = 0.004$, $n_1 = 0.613$, $n_2 = 6.439$, $k_2 = 2.21$, $k_3 = 0.19$)

It can be mentioned that more stretched particles having lower SF (0.25–0.5) give a qualitatively different profile compared to particles having a shape closer to spherical (1–0.75). It is also quantitatively reflected on the relative dimensionless erosion rate presented in table 4. Evidently, the same behavior would be observed for other empirical erosion models.

Table 4

“Shape factor” and erosion rate (ER)

Shape factor	ER
0.25	0.00349
0.5	0.0055466
0.75	0.0061866

Obviously, such a behavior is due to the change of particle velocity profile and the redistribution of particles having different sizes along the crater radii. The distributions of particle velocities and sizes, cell-averaged, for SF 0.25; 0.5; 0.75 are shown in fig. 15 and fig. 16. It can be seen that while SF decreases, the absolute velocity along the crater radii decreases slowly for $SF=0.5$ and more rapidly for $SF=0.25$, which follows the decrease of dimensionless erosion rate. Notable is also the change in profile shape: a drastic velocity decrease can be seen for $SF=0.25$ along the first 0.25 mm of crater radii. To the opposite, a smooth velocity decay is observed for $SF=0.75$ (having even a local increase). Decreasing SF leads to increase of the cell averaged diameter in the crater center vicinity, also followed by the growth of the cell-averaged diameters difference between the central and peripheral crater area. This also leads to the influence of averaged diameter local maximums for SF 0.75 and 0.5.

Fig. 17 shows the abrasive powder. The shape factor is obviously depending on the surface area of a particle and, therefore, some relation between the sides and/or perimeter of a particle. It can be supposed that for most particles, despite angularities and some coagulated large structures, such relation, if expressed as an aspect ratio, would be no higher than 0.4–0.5. An estimate made using free *ImageJ* software [40] for the relation of a circle with area equivalent to the summary area of particles to the summary perimeter of particles showed a value of ≈ 0.35 . Also, a qualitative similarity can be observed between the calculated erosion rate profile and experimental crater profile for shape factor 0.5 and lower. Therefore, using dimensionless erosion rate (table 2) and erosion rate profiles (fig. 13) the best agreement with experimental data is reached for $SF \approx 0.25$ and *Oka* erosion model with $E_{90} = 0.004$, $n_1 = 0.613$; $n_2 = 6.439$; $k_2 = 2.21$; $k_3 = 0.19$.

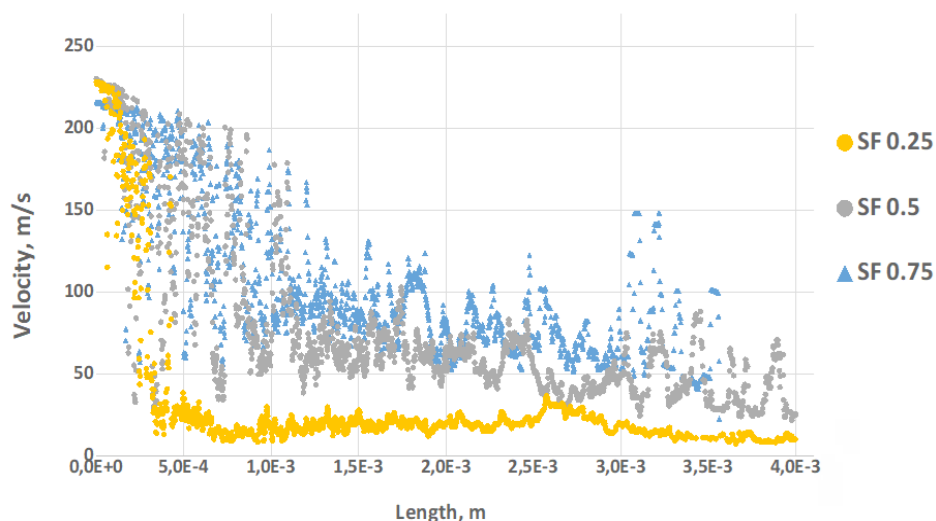


Fig. 15. Particle velocity near the sample wall along its length

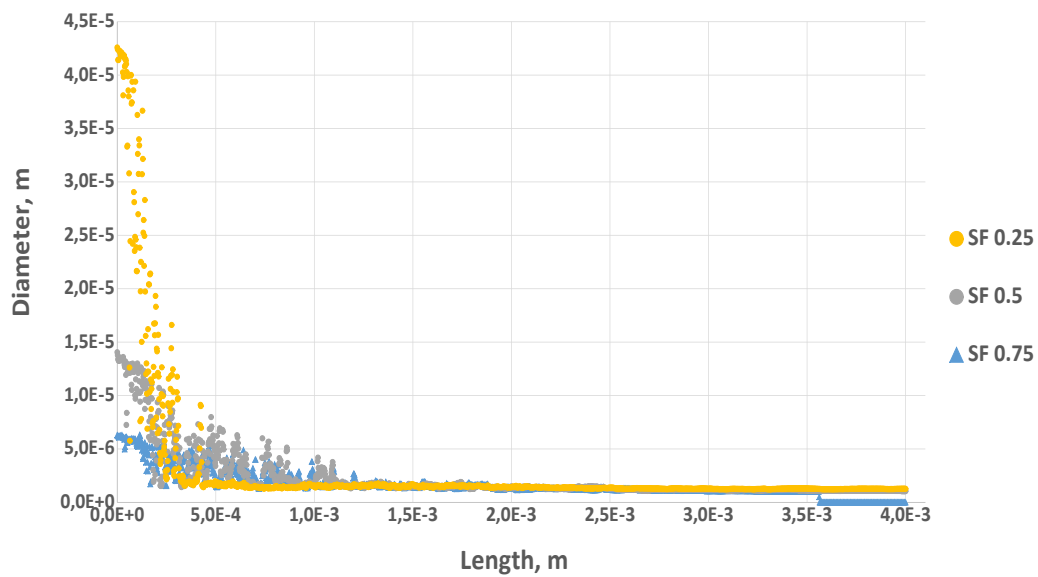


Fig. 16. Average particle diameter distribution near the sample wall along its length

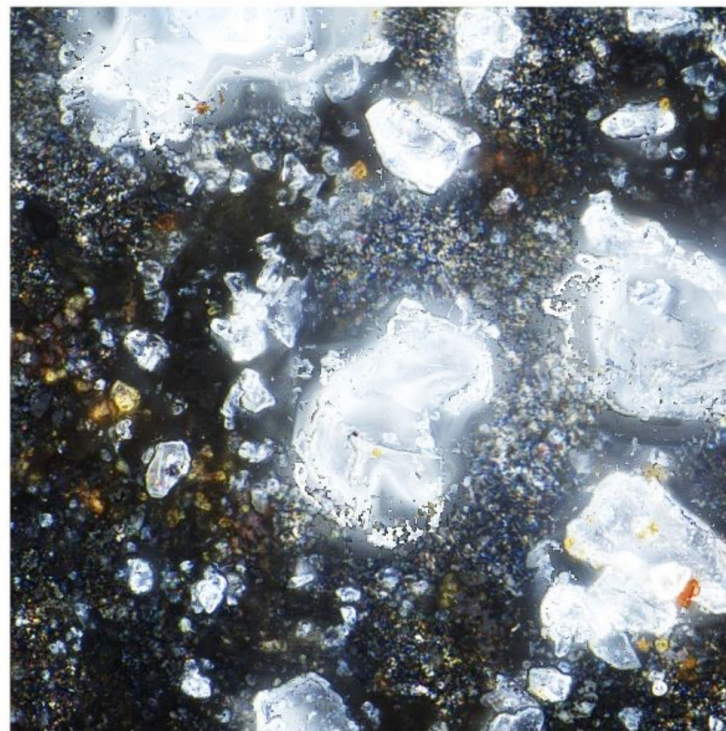


Fig. 17. A micrograph of erodent particles (quartz particles)

As is shown, erosion rate is independent of the turbulence model and its parameter choice at least for the studied conditions, and, oppositely, has a high dependence on the particle shape. This shows a need for more attention to the parameters of particles in contrast to the carrier flow modeling parameters. In future additional research should be carried on the effects of particle rotation, other particles distributions, angularity of particles and particles interactions – collisions, fracture and coalescence.

As shown before, *CFD* modeling of erosion process accounting for particle shapes can allow to predict and manage erosion rate on the treated surface. This might be useful for managing the erosive wear location and amplitude in machinery parts and also for working of metals during peening and peen forming processes.



Finally, future work should be reasonably conducted together with finite element analysis on local level to explicitly study particle-particle and particle-surface interactions and consider material properties in details. Such studies will be needed also for the estimation of erosion resistance of different types of coatings.

Conclusions

The numerical study made it possible to determine that:

1. The described approach allows to obtain a good agreement with the qualitative experimental data expressed in erosion crater profile and quantitatively, compared by integral non-dimensional erosion rate values for the studied conditions.

2. The calculated erosion rate under high-speed normal particles impact weakly depends on the turbulence model choice, including *GEKO* and its parameters;

3. On the contrary, the calculated wear rate significantly depends on the empirical erosion model choice and its calibrating coefficients.

4. The erosion rate profile and integral erosion rate are highly affected by the particle shape. The growth of drag due to change of the particle shapes leads to erosion rate decrease. For the studied conditions, shape factor values of ≈ 0.25 give the best agreement with the experimental data qualitatively and quantitatively.

References

1. Shinde S.M., Kawadekar D.M., Patil P.A., Bhojwani V.K. Analysis of micro and nano particle erosion by analytical, numerical and experimental methods: A review. *Journal of Mechanical Science and Technology*, 2019, vol. 33 (5), pp. 2319–2329. DOI: 10.1007/s12206-019-0431-x.
2. Hadziahmetovic H.D., Hodzic N., Kahrmanovic D., Dzaferovic E. Computational fluid dynamics (CFD) based erosion prediction model in elbows. *Tehnicki vjesnik = Technical Gazette*, 2014, vol. 21 (2), pp. 275–282.
3. Sun K., Lu L., Jin H. Modeling and numerical analysis of the solid particle erosion in curved ducts. *Abstract and Applied Analysis*, 2013, vol. 2013, art. 245074. DOI: 10.1155/2013/245074.
4. Finnie I. Erosion of surfaces by solid particles. *Wear*, 1960, vol. 3 (2), pp. 87–103. DOI: 10.1016/0043-1648(60)90055-7.
5. Grant G., Ball R., Tabakoff W. *An experimental study of the erosion rebound characteristics of high-speed particles impacting a stationary specimen*. Report No. 73-36. Cincinnati University Ohio, Department of Aerospace Engineering, 1973.
6. Bitter J.G.A. A study of erosion phenomena: Part I. *Wear*, 1963, vol. 6 (1), pp. 5–21. DOI: 10.1016/0043-1648(63)90003-6.
7. Bitter J.G.A. A study of erosion phenomena: Part II. *Wear*, 1963, vol. 6 (3), pp. 169–190. DOI: 10.1016/0043-1648(63)90073-5.
8. Strokach E.A., Kozhevnikov G.D., Pozhidaev A.A. Chislennoe modelirovanie protsessa erodirovaniya tverdy-mi chastitsami v gazovom potoke (obzor) [Numerical simulation of solid particle erosion in a gaseous flow (review)]. *Vestnik Permskogo natsional'nogo issledovatel'skogo politekhnicheskogo universiteta. Aerokosmicheskaya tekhnika = PNRPU Aerospace Engineering Bulletin*, 2021, no. 67, pp. 56–69. DOI: 10.15593.2224-9982.2021.67.06.
9. Tarodiya R., Levy A. Surface erosion due to particle-surface interactions – A review. *Powder Technology*, 2021, vol. 387, pp. 527–559. DOI: 10.1016/j.powtec.2021.04.055.
10. Krella A. Resistance of PVD coatings to erosive and wear processes: A review. *Coatings*, 2020, vol. 10, p. 921. DOI: 10.3390/coatings10100921.
11. Fardan A., Berndt C.C., Ahmed R. Numerical modelling of particle impact and residual stresses in cold sprayed coatings: A review. *Surface and Coatings Technology*, 2021, vol. 409. DOI: 10.1016/j.surfcoat.2021.126835.
12. Bonu V., Barshilia H.C. High-temperature solid particle erosion of aerospace components: its mitigation using advanced nanostructured coating technologies. *Coatings*, 2022, vol. 12, p. 1979. DOI: 10.3390/coatings12121979.
13. Taherkhani B., Anaraki A.P., Kadkhodapour J., Farahani N.K., Tu H. Erosion due to solid particle impact on the turbine blade: experiment and simulation. *Journal of Failure Analysis and Prevention*, 2019, vol. 19 (6), pp. 1739–1744. DOI: 10.1007/s11668-019-00775-y.



14. Khoddami A.S., Salimi-Majd D., Mohammadi B. Finite element and experimental investigation of multiple solid particle erosion on Ti–6Al–4V titanium alloy coated by multilayer wear-resistant coating. *Surface and Coatings Technology*, 2019, vol. 372 (2), pp. 173–189. DOI: 10.1016/j.surfcoat.2019.05.042.
15. Farokhipour A., Mansoori Z., Saffar-Avval M., Ahmadi G. Numerical modeling of sand particle erosion at return bends in gas-particle two-phase flow. *Scientia Iranica*, 2018, vol. 25 (6), pp. 3231–3242. DOI: 10.24200/sci.2018.50801.1871.
16. Peng S., Chen Q., Shan C., Wang D. Numerical analysis of particle erosion in the rectifying plate system during shale gas extraction. *Energy Science & Engineering*, 2019, vol. 7 (5), pp. 1838–1851. DOI: 10.1002/ese3.395.
17. Anielli D., Borello D., Rispoli F., Salvagni A., Venturini P. Prediction of particle erosion in the internal cooling channels of a turbine blade. *11th European Turbomachinery Conference*, 23 March 2015, Madrid, Spain, pp. 1–11.
18. Campos-Amezcuca A., Mazur Z., Gallegos-Muñoz A., Romero-Colmenero A., Manuel Riesco-Ávila J., Martín Medina-Flores J. Numerical study of erosion due to solid particles in steam turbine blades. *Numerical Heat Transfer, Part A: Applications*, 2008, vol. 53 (6), pp. 667–684. DOI: 10.1080/10407780701453933.
19. Arabnejad H. *Development of erosion equations for solid particle and liquid droplet impact*. Ph.D. diss. Department of Mechanical Engineering, The University of Tulsa, 2015. 161 p.
20. Mansouri A. *A combined CFD-experimental method for developing an erosion equation for both gas-sand and liquid-sand flows*. Ph.D. diss. Department of Mechanical Engineering, The University of Tulsa, 2016. 217 p.
21. Liu Y., Cao Z., Yuan J., Sun X., Su H., Wang L. Effect of morphology, impact velocity and angle of the CaO-MgO-Al₂O₃-SiO₂ (CMAS) particle on the erosion behavior of thermal barrier coatings (TBCs): a finite element simulation study. *Coatings*, 2022, vol. 12 (5), p. 576. DOI: 10.3390/coatings12050576.
22. Ma Z.S., Fu L.H., Yang L., Zhou Y.C., Lu C. Finite element simulations on erosion and crack propagation in thermal barrier coatings. *High Temperature Materials and Processes*, 2015, vol. 34 (4), pp. 387–393. DOI: 10.1515/htmp-2014-0068.
23. Liu Z.G., Wan S., Nguyen V.B., Zhang Y.W. Finite element analysis of erosive wear for offshore structure. *13th International Conference on Fracture*, 16–21 June 2013, Beijing, China, pp. 461–468.
24. Oviedo F., Valarezo A. Residual stress in high-velocity impact coatings: parametric finite element analysis approach. *Journal of Thermal Spray Technology*, 2020, vol. 29 (6), pp. 1268–1288. DOI: 10.1007/s11666-020-01026-5.
25. Bing Wu, Fengfang Wu, Jinjie Li. Finite element modeling of correlating mechanical properties with erosion wear rate. *Proceedings of the 2018 3rd International Conference on Electrical, Automation and Mechanical Engineering (EAME 2018)*, June 2018. Atlantis press, 2018, pp. 273–276. DOI: 10.2991/eame-18.2018.57.
26. Singh P.K., Hota A.R., Mishra S.B. Finite element modelling of erosion parameters in Bing boiler components. *Asian Journal of Engineering and Applied Technology*, 2018, vol. 7 (2), pp. 12–16. DOI: 10.51983/ajeat-2018.7.2.964.
27. Dong X., Li Z., Feng L., Sun Z., Fan C. Modeling, simulation, and analysis of the impact(s) of single angular-type particles on ductile surfaces using smoothed particle hydrodynamics. *Powder Technology*, 2017, vol. 318, pp. 363–382. DOI: 10.1016/j.powtec.2017.06.011.
28. Leguizamón S., Jahanbakhsh E., Alimirzazadeh S., Maertens A., Avellan F. FVPM numerical simulation of the effect of particle shape and elasticity on impact erosion. *Wear*, 2019, vol. 430–431, pp. 108–119. DOI: 10.1016/j.wear.2019.04.023.
29. Menter F., Lechner R., Matyushenko A. *Best practice: generalized K- Ω two-equation turbulence model in ANSYS CFD (GEKO)*. Technical Report ANSYS. Nurnberg, Germany, 2019. 32 p.
30. *ANSYS Fluent Theory Guide*. Canonsburg, PA, ANSYS Inc, 2019. 1080 p.
31. Menter F.R., Matyushenko A., Lechner R. Development of a generalized K- ω two-equation turbulence model. *Notes on Numerical Fluid Mechanics and Multidisciplinary Design*, 2018, vol. 142, pp. 101–109. DOI: 10.1007/978-3-030-25253-3_10.
32. Strokach E., Zhukov V., Borovik I., Sternin A., Haidn O.J. Simulation of a GOx-gch4 rocket combustor and the effect of the GEKO turbulence model coefficients. *Aerospace*, 2021, vol. 8 (11), p. 341. DOI: 10.3390/aerospace8110341.
33. Pozhidaev A., Kozhevnikov G., Strokach E. Numerical study of turbulence model effect on solid particle erosion in gaseous flow. *AIP Conference Proceedings*, 2023, vol. 2549 (1), p. 030003. DOI: 10.1063/5.0130489.
34. Oka Y.I., Ohnogi H., Hosokawa T., Matsumura M. The impact angle dependence of erosion damage caused by solid particle impact. *Wear*, 1997, vol. 203–204, pp. 573–579. DOI: 10.1016/s0043-1648(96)07430-3.
35. Haugen K., Kvernfold O., Ronold A., Sandberg R. Sand erosion of wear resistant materials: Erosion in choke valves. *Wear*, 1995, vol. 186–187, pp. 179–188. DOI: 10.1016/0043-1648(95)07158-X.



36. Duarte Ribeiro C.A., Souza F., Salvo R., Santos V. The role of inter-particle collisions on elbow erosion. *International Journal of Multiphase Flow*, 2016, vol. 89, pp. 1–22. DOI: 10.1016/j.ijmultiphaseflow.2016.10.001.
37. *Recommended practice RP O501 Erosive wear in piping systems*. Revision 4.2-2007 (DNV RP O501 – Revision 4.2-2007). Det Norske Veritas, 2007. 43 p.
38. Haider A., Levenspiel O. Drag coefficient and terminal velocity of spherical and nonspherical particles. *Powder Technology*, 1989, vol. 58 (1), pp. 63–70. DOI: 10.1016/0032-5910(89)80008-7.
39. Morsi S.A., Alexander A.J. An investigation of particle trajectories in two-phase flow systems. *Journal of Fluid Mechanics*, 1972, vol. 55, pt. 2, pp. 193–208. DOI: 10.1017/s0022112072001806.
40. *ImageJ. Image Processing and Analysis in Java*. Available at: <https://imagej.net/ij/index.html> (accessed 31.10.2023).

Conflicts of Interest

The authors declare no conflict of interest.

© 2023 The Authors. Published by Novosibirsk State Technical University. This is an open access article under the CC BY license (<http://creativecommons.org/licenses/by/4.0>).

